Spin density matrix of top quark pairs produced in electron-positron annihilation including QCD radiative corrections

Arnd Brandenburg, Marc Flesch, and Peter Uwer
Institut für Theoretische Physik, RWTH Aachen, D-52056 Aachen, Germany
(Received 9 June 1998; published 13 November 1998)

We calculate the spin density matrix of top quark pairs for the reaction $e^+e^-\to t\bar{t}X$ to order α_s. As an application we show next-to-leading order results for a variety of spin observables for the $t\bar{t}$ system. These include the top quark and antiquark polarizations and $t\bar{t}$ spin-spin correlations as a function of the center-of-mass energy and of the top quark scattering angle for arbitrary longitudinal polarization of the electron-positron beam. [S0556-2821(98)00423-8]

PACS number(s): 14.65.Ha, 12.38.Bx, 13.88.+e

I. INTRODUCTION

Among the six known quark flavors known to date, the top quark is of particular interest: Its large mass implies that very high energies are involved in the production and decay of this particle, which in turn allows for tests of the fundamental interactions at these high energy scales. Moreover, the interactions of the top quark can be studied in greater detail than those of the lighter particles since the top quark essentially behaves like a free, but extremely short-lived, particle. With a mass of $m\approx 175$ GeV, the lifetime of the top quark is about 5×10^{-25} s. This short lifetime effectively cuts off the long distance QCD dynamics. In particular, the top quark polarization is not diluted by hadronization and thus becomes an additional observable to test perturbative QCD or, more generally, short distance physics.

An ideal machine to study the properties of top quarks in detail would be a high-luminosity, high-energetic e^+e^- linear collider. The physics potential of such a machine is described for example in [1]. We just mention here that at center-of-mass energies in the range $\sqrt{s}=400-1000$ GeV, an annual yield of the order of 10^5 top quark pairs may be expected.

For the process $e^+e^-\to t\bar{t}X$, a detailed analysis of top quark spin effects has been performed in the Born approximation in [2]. Recently, the correlations between the spins of top quarks and antiquarks have been studied extensively in leading order also in [3]. The production cross sections for top quarks with longitudinal [4], transverse [5], and transverse normal [2,6] polarization are known to order α_s. The *longitudinal* spin-spin correlations have also been calculated in next-to-leading order (NLO) [7,8]. Polarization phenomena in top quark pair production near threshold have been investigated in [9].

A convenient theoretical framework to discuss spin phenomena is the concept of the spin density matrix, and the main objective of this paper is to present results for the full spin density matrix of the $t\bar{t}$ system to order α_s. This allows for a systematic study of spin effects in $e^+e^-\to t\bar{t}X$. For phenomenological applications, our results should be supplemented by the decay matrices at NLO for the different t and $\bar{t}$ decay channels [10,11].

An alternative approach to the analysis of spin effects in top quark production and decay is the computation of the relevant helicity amplitudes. This was accomplished at next-to-leading order in [12], where also a Monte Carlo event generator for the case of semileptonic $t\bar{t}$ decays was constructed.

The outline of the rest of this paper is as follows. We start in Sec. II by introducing the spin density matrix formalism and apply it to the reaction $e^+e^-\to t\bar{t}$ at leading order. In Sec. III we compute the QCD radiative corrections to the results of Sec. II. Section IV contains numerical results for a variety of spin observables. We exhibit their dependence on the c.m. energy and on the top quark scattering angle and further study the effects of electron beam polarization.

II. KINEMATICS AND LEADING ORDER RESULTS

In this section we review some basic kinematics and the concept of the spin density matrix formalism. To set up the notation, we start with a closer look at the amplitude for the process

$$e^+(p_+)e^-(p_-)\to(\gamma^*,Z^*)\to t(k_t)\bar{t}(k_{\bar{t}})X, \qquad (2.1)$$

where $e^-(e^+)$ denotes an electron (positron) and $t(\bar{t})$ describes a top (anti-)quark with mass m. We work in leading order in the electroweak coupling and in next-to-leading order in the strong coupling $\alpha_s=g_s^2/(4\pi)$. To this order the unspecified rest X can be only a gluon. The amplitude for the reaction (2.1) can be written in the following form:

$$\mathcal{T}_{fi}=\frac{4\pi\alpha}{s}\{\chi(s)\bar{v}(p_+)(g_v^e\gamma_\mu-g_a^e\gamma_\mu\gamma_5)u(p_-)\times(g_v^tV^\mu-g_a^tA^\mu)+\bar{v}(p_+)\gamma_\mu u(p_-)(-Q_tV^\mu)\}. \qquad (2.2)$$

In Eq. (2.2), $s=(p_++p_-)^2$, Q_t denotes the electric charge of the top quark in units of $e=\sqrt{4\pi\alpha}$, and g_v^f, g_a^f are the vector- and the axial-vector couplings of a fermion of type f, i.e.

$$g_v^f = T_3^f - 2Q_f \sin^2\vartheta_W \tag{2.3}$$

and

$$g_a^f = T_3^f, \tag{2.4}$$

in particular $g_v^e = -\frac{1}{2} + 2\sin^2\vartheta_W$, $g_a^e = -\frac{1}{2}$ for an electron, and $g_v^t = \frac{1}{2} - \frac{4}{3}\sin^2\vartheta_W$, $g_a^t = \frac{1}{2}$ for a top quark, with ϑ_W denoting the weak mixing angle. The function $\chi(s)$ is given by

$$\chi(s) = \frac{1}{4\sin^2\vartheta_W \cos^2\vartheta_W} \frac{s}{s - m_Z^2 + i m_Z \Gamma_Z}, \tag{2.5}$$

where m_Z and Γ_Z stand for the mass and the width of the Z boson. (We keep here the width of the Z boson because it will be relevant for an application of our results to b quark production at the Z resonance.) The amplitudes V_μ, A_μ in Eq. (2.2) encode information on the decay of the vector boson into the $t\bar{t}$ and $t\bar{t}g$ final states. In particular they depend on the momentum and the polarization of the outgoing particles. Considering only longitudinal polarization for the incoming electrons and/or positrons and neglecting the lepton masses leads to

$$|\mathcal{T}_{fi}|^2 = \frac{16\pi^2\alpha^2}{s^2}[L^{PC\mu\nu} H^{PC}_{\mu\nu} + L^{PV\mu\nu} H^{PV}_{\mu\nu}] \tag{2.6}$$

for the square of Eq. (2.2). The lepton tensors $L^{PC(PV)\mu\nu}$ read

$$L^{PC\mu\nu} = p_+^\mu p_-^\nu + p_+^\nu p_-^\mu - g^{\mu\nu} p_+ p_- \tag{2.7}$$

and

$$L^{PV\mu\nu} = -i\varepsilon^{\mu\nu}_{\rho\sigma} p_+^\rho p_-^\sigma . \tag{2.8}$$

The tensors $H^{PC(PV)}_{\mu\nu}$ describing the decay of a polarized Z boson can be written as

$$H^{PC(PV)}_{\mu\nu} = g^{VV}_{PC(PV)} H^{VV}_{\mu\nu} + g^{AA}_{PC(PV)} H^{AA}_{\mu\nu} + g^{VA_+}_{PC(PV)} H^{VA_+}_{\mu\nu} + g^{VA_-}_{PC(PV)} H^{VA_-}_{\mu\nu}, \tag{2.9}$$

with

$$H^{VV}_{\mu\nu} = V_\mu V_\nu^* , \tag{2.10}$$

$$H^{AA}_{\mu\nu} = A_\mu A_\nu^* , \tag{2.11}$$

and

$$H^{VA_\pm}_{\mu\nu} = V_\mu A_\nu^* \pm A_\mu V_\nu^* . \tag{2.12}$$

The couplings g_X^Y $(X \in \{PC, PV\},\ Y \in \{VV, AA, VA_+, VA_-\})$ in Eq. (2.9) are given by

$$g^{VV}_{PC(PV)} = Q_t^2 f^{\gamma\gamma}_{PC(PV)} + 2 g_v^t Q_t \mathrm{Re}\chi(s)\ f^{\gamma Z}_{PC(PV)} + g_v^{t2} |\chi(s)|^2 f^{ZZ}_{PC(PV)}, \tag{2.13}$$

$$g^{AA}_{PC(PV)} = g_a^{t2} |\chi(s)|^2 f^{ZZ}_{PC(PV)}, \tag{2.14}$$

$$g^{VA_+}_{PC(PV)} = -g_a^t Q_t \mathrm{Re}\chi(s)\ f^{\gamma Z}_{PC(PV)} - g_v^t g_a^t |\chi(s)|^2 f^{ZZ}_{PC(PV)}, \tag{2.15}$$

$$g^{VA_-}_{PC(PV)} = i g_a^t Q_t \mathrm{Im}\chi(s)\ f^{\gamma Z}_{PC(PV)}, \tag{2.16}$$

where

$$f^{ZZ}_{PC} = (1 - \lambda_- \lambda_+)(g_v^{e2} + g_a^{e2}) - 2(\lambda_- - \lambda_+) g_v^e g_a^e, \tag{2.17}$$

$$f^{\gamma\gamma}_{PC} = 1 - \lambda_- \lambda_+ , \tag{2.18}$$

$$f^{ZZ}_{PV} = (\lambda_- - \lambda_+)(g_v^{e2} + g_a^{e2}) - 2(1 - \lambda_- \lambda_+) g_v^e g_a^e, \tag{2.19}$$

$$f^{\gamma\gamma}_{PV} = \lambda_- - \lambda_+ , \tag{2.20}$$

$$f^{\gamma Z}_{PC} = -(1 - \lambda_- \lambda_+) g_v^e + (\lambda_- - \lambda_+) g_a^e, \tag{2.21}$$

$$f^{\gamma Z}_{PV} = (1 - \lambda_- \lambda_+) g_a^e - (\lambda_- - \lambda_+) g_v^e, \tag{2.22}$$

with λ_- (λ_+) denoting the longitudinal polarization of the electron (positron) beam.[1] The couplings $g^{VA_-}_{PC(PV)}$ are formally of higher order in the electroweak couplings. The structure $H^{VA_-}_{\mu\nu}$ will therefore not be discussed further. For top quark production, where $\sqrt{s} \gg m_Z$, one should set the width Γ_Z of the Z boson to zero for consistency.

The (unnormalized) spin density matrix for the reaction (2.1) may be defined by

$$\rho_{\alpha\alpha',\beta\beta'} = \widehat{\sum} \langle t(k_t,\alpha)\bar{t}(k_{\bar{t}},\alpha') X | \mathcal{T} | e^+(p_+,\lambda_+) e^-(p_-,\lambda_-)\rangle \times \langle t(k_t,\beta)\bar{t}(k_{\bar{t}},\beta') X | \mathcal{T} | e^+(p_+,\lambda_+) e^-(p_-,\lambda_-)\rangle^*, \tag{2.23}$$

where $\alpha, \alpha', \beta, \beta'$ are the spin indices of the outgoing top (anti-)quarks. The sum $\hat{\Sigma}$ in Eq. (2.23) runs over all unobserved degrees of freedom such as the color of the outgoing particles or the polarization of the emitted gluon. In Eq. (2.23) one should read the combination $\alpha\alpha'$ $(\beta\beta')$ on the left-hand side as a shorthand notation for a multi-index built

[1] For a right-handed electron (positron), $\lambda_\mp = +1$.

from α,α' (β,β'). To calculate the spin density matrix it is convenient to use a different representation which follows immediately from the concept of the density matrix:

$$\widehat{\sum}|\mathcal{T}(e^+(p_+,\lambda_+)e^-(p_-,\lambda_-)\to t(k_t,\hat{\mathbf{s}}_t)\bar{t}(k_{\bar{t}},\hat{\mathbf{s}}_{\bar{t}})X)|^2$$
$$=\mathrm{Tr}\left[\rho\frac{1}{2}(\mathbb{1}+\hat{\mathbf{s}}_t\cdot\boldsymbol{\sigma})\otimes\frac{1}{2}(\mathbb{1}+\hat{\mathbf{s}}_{\bar{t}}\cdot\boldsymbol{\sigma})\right]. \quad (2.24)$$

Here $\hat{\mathbf{s}}_t(\hat{\mathbf{s}}_{\bar{t}})$ is the unit polarization of the top (anti-)quark in the rest frame of the top (anti-)quark,[2] and σ_i are the usual Pauli matrices. With $\otimes$ we denote the tensor product between the spin space of the quark and the antiquark. Using in Eq. (2.24) a decomposition of the spin density matrix ρ of the form

$$\rho=a\mathbb{1}\otimes\mathbb{1}+\mathbf{B}^+\cdot\boldsymbol{\sigma}\otimes\mathbb{1}+\mathbb{1}\otimes\boldsymbol{\sigma}\cdot\mathbf{B}^-+C_{ij}\sigma_i\otimes\sigma_j, \quad (2.25)$$

the density matrix can be easily calculated by a comparison of the polarization independent parts, terms proportional to $\hat{\mathrm{s}}_{ti}$ $(\hat{\mathrm{s}}_{\bar{t}i})$, and terms proportional to $\hat{\mathrm{s}}_{ti}\hat{\mathrm{s}}_{\bar{t}j}$ on the left-hand side and the right-hand side of Eq. (2.24). More precisely we define

$$\rho=4\pi^2\alpha^2N_C\sum_{Y,X}g_X^Y\rho_Y^X \quad (2.26)$$

$(X\in\{PC,PV\},\ Y\in\{VV,AA,VA_+\})$, with

$$\mathrm{Tr}\left[\rho_Y^X\frac{1}{2}(\mathbb{1}+\hat{\mathbf{s}}_t\cdot\boldsymbol{\sigma})\otimes\frac{1}{2}(\mathbb{1}+\hat{\mathbf{s}}_{\bar{t}}\cdot\boldsymbol{\sigma})\right]=\frac{1}{N_C}\frac{4}{s^2}\widehat{\sum}L^{X\mu\nu}H^Y_{\mu\nu}, \quad (2.27)$$

where N_C is the number of colors, and g_X^Y are the couplings as given in Eqs. (2.13)–(2.16). For the density matrices ρ_Y^X we use a representation as in Eq. (2.25). It is useful to decompose the polarizations $\mathbf{B}_Y^{X,\pm}$ and the spin-spin correlations $C_{Y,ij}^X$ further. For the two-parton final state it is convenient to write

$$\mathbf{B}^\pm=b_1^\pm\hat{\mathbf{p}}+b_2^\pm\hat{\mathbf{k}}+b_3^\pm\hat{\mathbf{n}},$$

$$C_{ij}=c_0\delta_{ij}+\varepsilon_{ijk}(c_1\hat{\mathrm{p}}_k+c_2\hat{\mathrm{k}}_k+c_3\hat{\mathrm{n}}_k)$$
$$+c_4\hat{\mathrm{p}}_i\hat{\mathrm{p}}_j+c_5\hat{\mathrm{k}}_i\hat{\mathrm{k}}_j$$
$$+c_6(\hat{\mathrm{p}}_i\hat{\mathrm{k}}_j+\hat{\mathrm{p}}_j\hat{\mathrm{k}}_i)+c_7(\hat{\mathrm{p}}_i\hat{\mathrm{n}}_j+\hat{\mathrm{p}}_j\hat{\mathrm{n}}_i)$$
$$+c_8(\hat{\mathrm{k}}_i\hat{\mathrm{n}}_j+\hat{\mathrm{k}}_j\hat{\mathrm{n}}_i), \quad (2.28)$$

with

$$\hat{\mathbf{p}}=\frac{\mathbf{p}_-}{|\mathbf{p}_-|}, \quad (2.29)$$

$$\hat{\mathbf{k}}=\frac{\mathbf{k}_t}{|\mathbf{k}_t|}, \quad (2.30)$$

$$\hat{\mathbf{n}}=\frac{\hat{\mathbf{p}}\times\hat{\mathbf{k}}}{|\hat{\mathbf{p}}\times\hat{\mathbf{k}}|}, \quad (2.31)$$

where the three-momenta $\mathbf{p}$ and $\mathbf{k}$ are defined in e^+e^- c.m. system. In Eq. (2.28) we suppress for simplicity the additional indices Y,X. For the case of the three-parton final state a similar decomposition can be used. A detailed discussion of the properties of ρ under discrete symmetry transformations is given in [13]. In leading order $[O(\alpha_s^0)]$ the nonvanishing entries in the density matrices ρ_Y^X read

$$a_{VV}^{PC}=2-\beta^2(1-z^2), \quad (2.32)$$

$$c_{0,VV}^{PC}=-\beta^2(1-z^2), \quad (2.33)$$

$$c_{4,VV}^{PC}=2, \quad (2.34)$$

$$c_{5,VV}^{PC}=2[(1-r)^2z^2+\beta^2], \quad (2.35)$$

$$c_{6,VV}^{PC}=-2(1-r)z, \quad (2.36)$$

$$b_{1,VV}^{\pm,PV}=2r, \quad (2.37)$$

$$b_{2,VV}^{\pm,PV}=2(1-r)z, \quad (2.38)$$

$$a_{AA}^{PC}=\beta^2(1+z^2), \quad (2.39)$$

$$c_{0,AA}^{PC}=\beta^2(1-z^2), \quad (2.40)$$

$$c_{4,AA}^{PC}=-2\beta^2, \quad (2.41)$$

$$c_{6,AA}^{PC}=2\beta^2z, \quad (2.42)$$

$$b_{2,AA}^{\pm,PV}=2\beta^2z, \quad (2.43)$$

$$b_{1,VA_+}^{\pm,PC}=2\beta rz, \quad (2.44)$$

$$b_{2,VA_+}^{\pm,PC}=2\beta[1+(1-r)z^2], \quad (2.45)$$

$$a_{VA_+}^{PV}=4\beta z, \quad (2.46)$$

[2]We define the rest frame of the outgoing top (anti-)quark as the rest system which is obtained by a rotation-free Lorentz-boost from the center-of-mass system of the e^+e^--pair.

$$c_{5,VA_+}^{PV}=4\beta(1-r)z, \tag{2.47}$$

$$c_{6,VA_+}^{PV}=2\beta r, \tag{2.48}$$

where $z=\hat{\mathbf{p}}\cdot\hat{\mathbf{k}}$, $\beta=\sqrt{1-4m^2/s}$, and $r=2m/\sqrt{s}$ is the scaled top quark mass.[3]

The leading order differential cross section $d\sigma_0(\hat{\mathbf{s}}_t,\hat{\mathbf{s}}_{\bar{t}})$ is related to the leading order density matrix ρ_0 as follows:

$$d\sigma(\hat{\mathbf{s}}_t,\hat{\mathbf{s}}_{\bar{t}})=\frac{1}{2s}\,\mathrm{Tr}\left[\rho_0\frac{1}{2}(\mathbb{1}+\hat{\mathbf{s}}_t\cdot\boldsymbol{\sigma})\otimes\frac{1}{2}(\mathbb{1}+\hat{\mathbf{s}}_{\bar{t}}\cdot\boldsymbol{\sigma})\right]dR_2, \tag{2.49}$$

with

$$dR_2=\frac{d^3k_t}{(2\pi)^3 2k_t^0}\,\frac{d^3k_{\bar{t}}}{(2\pi)^3 2k_{\bar{t}}^0}(2\pi)^4\delta(p_+ + p_- - k_t - k_{\bar{t}}). \tag{2.50}$$

The total cross section for example can be obtained from

$$\sigma_0=\frac{1}{2s}\,\frac{\beta}{16\pi}\int_{-1}^{1}dz\ \mathrm{Tr}[\rho_0]$$
$$=\frac{1}{2s}\,\pi\alpha^2 N_C\beta\int_{-1}^{1}dz\,(g_{PC}^{VV}a_{VV}^{PC}+g_{PC}^{AA}a_{AA}^{PC}), \tag{2.51}$$

yielding the well-known result

$$\sigma_0=\sigma_{pt}N_C\beta\left(\frac{3-\beta^2}{2}g_{PC}^{VV}+\beta^2 g_{PC}^{AA}\right), \tag{2.52}$$

with

$$\sigma_{pt}=\frac{4\pi\alpha^2}{3s}. \tag{2.53}$$

Within the framework of the spin density matrix formalism it is easy to calculate spin observables. For instance, at leading order the polarization of the top quark projected onto its momentum direction can be obtained from

$$\langle\hat{\mathbf{k}}\cdot\mathbf{S}_t\rangle=\frac{\int_{-1}^{1}dz\ \mathrm{Tr}\left[\rho_0\left(\hat{\mathbf{k}}\cdot\frac{\boldsymbol{\sigma}}{2}\otimes\mathbb{1}\right)\right]}{\int_{-1}^{1}dz\ \mathrm{Tr}[\rho_0]}$$
$$=\frac{2\int_{-1}^{1}dz\,g_{PC}^{VA_+}(zb_{1,VA_+}^{+,PC}+b_{2,VA_+}^{+,PC})+g_{PV}^{VV}(zb_{1,VV}^{+,PV}+b_{2,VV}^{+,PV})+g_{PV}^{AA}b_{2,AA}^{+,PV}}{4\int_{-1}^{1}dz(g_{PC}^{VV}a_{VV}^{PC}+g_{PC}^{AA}a_{AA}^{PC})}$$
$$=\frac{2\beta g_{PC}^{VA_+}}{(3-\beta^2)g_{PC}^{VV}+2\beta^2 g_{PC}^{AA}}, \tag{2.54}$$

where $\mathbf{S}_t=(\boldsymbol{\sigma}/2)\otimes\mathbb{1}$ is the top quark spin operator. [The spin operator of the top antiquark is $\mathbf{S}_{\bar{t}}=\mathbb{1}\otimes(\boldsymbol{\sigma}/2)$.] As another example consider the following spin-spin correlation, which is in leading order proportional to the so-called longitudinal spin-spin correlation studied in [7,8]:

$$\langle(\hat{\mathbf{k}}\cdot\mathbf{S}_t)(\hat{\mathbf{k}}\cdot\mathbf{S}_{\bar{t}})\rangle=\frac{\int_{-1}^{1}dz\ \mathrm{Tr}\left[\rho_0\left(\hat{\mathbf{k}}\cdot\frac{\boldsymbol{\sigma}}{2}\otimes\hat{\mathbf{k}}\cdot\frac{\boldsymbol{\sigma}}{2}\right)\right]}{\int_{-1}^{1}dz\ \mathrm{Tr}[\rho_0]}$$
$$=\frac{1}{4}\,\frac{(1+\beta^2)g_{PC}^{VV}+2\beta^2 g_{PC}^{AA}}{(3-\beta^2)g_{PC}^{VV}+2\beta^2 g_{PC}^{AA}}. \tag{2.55}$$

The examples above show that the spin density matrix formalism enables one to calculate efficiently the expectation values of spin observables. A more exhaustive analysis of spin observables together with next-to-leading order numerical results will be presented in Sec. IV.

III. QCD RADIATIVE CORRECTIONS

The QCD corrections at order α_s to the expectation values of spin observables are given by the contributions from one-loop virtual corrections to $e^+e^-\to t\bar{t}$ and from the real gluon emission process $e^+e^-\to t\bar{t}g$ at leading order. We first give some details of the computation of the virtual corrections.

Both infrared (IR) and ultraviolet (UV) singularities which appear in the one-loop integrals of the virtual corrections are treated within the framework of dimensional regularization in $d=4-2\epsilon$ space-time dimensions. We use the 't Hooft–Veltman prescription [14] to treat the γ_5 matrix present in the axial vector current part of the vertex correction in d dimensions. It is well known that this prescription

[3]It is interesting to note that the above results remain unchanged in $d=4-2\epsilon$ space-time dimensions if one keeps the $Z(\gamma)$ polarization vector in 4 dimensions.

violates certain Ward identities. They are restored by adding a finite counterterm [15]. Note that no ambiguities arise from the IR poles of the loop integrals. This follows from the fact that the coefficient in front of the IR divergent scalar one-loop integral is independent of ϵ if the $Z(\gamma)$ polarization vector is kept in 4 dimensions.

The UV singularities are removed by appropriate counterterms fixed by on-shell renormalization conditions for the quark. After renormalization one obtains UV finite vertex corrections for the vector and the axial vector parts of the amplitude to order α_s.

The renormalized amplitude still contains an IR singularity which appears as a single pole in ϵ and which multiplies—up to a factor—the Born amplitude. This singularity is cancelled in infrared safe quantities by a corresponding singularity from the real gluon emission process. The latter singularity is obtained from the phase space integration of the squared matrix element for $e^+e^-\to t\bar{t}g$ over the region of phase space where the gluon is soft.

The virtual corrections to the density matrix are obtained by first computing the interference between the renormalized one-loop amplitude and the Born amplitude for given polarization vectors $\hat{\mathbf{s}}_t$, $\hat{\mathbf{s}}_{\bar{t}}$ and then extracting ρ^{virtual} as described in Sec. II below Eq. (2.24). Note that the necessary trace algebra can now be performed in $d=4$ dimensions. In particular, the projectors $(1+\gamma_5 \not{s}_{t,\bar{t}})/2$ can be kept in 4 dimensions.

We now discuss the contributions from real gluon emission. We isolate the soft gluon singularities by splitting the $t\bar{t}g$ phase space into a soft and a hard gluon region. The soft gluon region is defined by the condition

$$E_g \leqslant x_{\min}\frac{\sqrt{s}}{2}, \tag{3.1}$$

where E_g is the gluon energy in the c.m. system and $x_{\min}$ is a sufficiently small quantity. The hard gluon region is the complement of the soft region. In the limit where the gluon momentum k_g goes to zero one can neglect k_g in the numerator of $\mathcal{T}_{fi}(e^+e^-\to t\bar{t}g)$, which leads to

$$\rho(e^+e^-\to t\bar{t}g) \xrightarrow{k_g\to 0} 4\pi\alpha_s C_F\left\{\frac{2k_t k_{\bar{t}}}{(k_t k_g)(k_{\bar{t}}k_g)}-\frac{m^2}{(k_t k_g)^2}-\frac{m^2}{(k_{\bar{t}}k_g)^2}\right\}\rho_0(e^+e^-\to t\bar{t}). \tag{3.2}$$

Using Eq. (3.2) in the whole soft gluon region leads to the approximation

$$\int \frac{d^{d-1}k_g}{(2\pi)^{d-1}2E_g}\Theta\left(x_{\min}\frac{\sqrt{s}}{2}-E_g\right)\rho(e^+e^-\to t\bar{t}g)\approx S\rho_0(e^+e^-\to t\bar{t})\equiv\rho^{\text{soft}}, \tag{3.3}$$

where the soft factor S is given by

$$\begin{aligned}S&=4\pi\alpha_s C_F\int\frac{d^{d-1}k_g}{(2\pi)^{d-1}2E_g}\Theta\left(x_{\min}\frac{\sqrt{s}}{2}-E_g\right)\left\{\frac{2k_t k_{\bar{t}}}{(k_t k_g)(k_{\bar{t}}k_g)}-\frac{m^2}{(k_t k_g)^2}-\frac{m^2}{(k_{\bar{t}}k_g)^2}\right\}\\&=\frac{\alpha_s}{2\pi}C_F\frac{1}{\Gamma(1-\epsilon)}\left(\frac{4\pi\mu^2}{s}\right)^{\epsilon}(x_{\min}^2)^{-\epsilon}\frac{1}{\epsilon}\frac{1}{\beta}\left\{2\beta+(1+\beta^2)\ln(\omega)-2\epsilon\left[\ln(\omega)+(1+\beta^2)\left(\text{Li}_2(1-\omega)+\frac{1}{4}\ln^2(\omega)\right)\right]\right\}+\mathcal{O}(\epsilon).\end{aligned} \tag{3.4}$$

Here, $C_F=(N_C^2-1)/(2N_C)$, $\beta=\sqrt{1-4m^2/s}$, and $\omega=(1-\beta)/(1+\beta)$. The scale μ is introduced in Eq. (3.4) to keep the strong coupling constant dimensionless in d dimensions. The dependence on μ cancels in the sum of the virtual and soft contributions.[4]

For finite $x_{\min}$, the sum of the contributions from the soft and hard gluon region differs from the exact result by terms of order $x_{\min}$ because of the soft gluon approximation. The sum becomes exact for $x_{\min}\to 0$. With the choice $x_{\min}=10^{-5}$ the systematic error due to this approximation is smaller than 1 per mil in all our numerical results. This can be nicely checked by varying $x_{\min}$ between, say, 10^{-3} and 10^{-6} and numerically extrapolating to zero.

The sum of the virtual and soft contributions to the density matrix ρ is finite and can be written in a compact form as follows:

We define

$$\begin{aligned}L=-\frac{\alpha_s}{2\pi}C_F\frac{1}{\beta}\Bigg\{&[2\beta+(1+\beta^2)\ln(\omega)]\\&\times\left[\ln(x_{\min}^2)-\ln\left(\frac{1-\beta^2}{4}\right)+2\right]\\&+(1+\beta^2)[4\text{Li}_2(1-\omega)+\ln^2(\omega)-\pi^2]\Bigg\},\end{aligned} \tag{3.5}$$

[4]Note that the leading order density matrix ρ_0 in Eq. (3.2) does not depend on ϵ (cf. footnote 3). Therefore, no additional finite terms are generated when multiplying the pole in ϵ of the soft factor S with ρ_0. In particular, no spurious terms due to the presence of γ_5 arise in the soft region.

and use as further abbreviations

$$\kappa=\frac{\alpha_s}{2\pi}C_F, \tag{3.6}$$

$$l_1=-\kappa\beta\,\ln(\omega), \tag{3.7}$$

$$l_2=(2-\beta^2)l_1, \tag{3.8}$$

$$l_3=\frac{1}{\beta}\,l_1. \tag{3.9}$$

Then,

$$\lim_{\epsilon\to 0}(\rho^{\text{virtual}}+\rho^{\text{soft}})=L\rho_0+\rho^{\text{rest}}, \tag{3.10}$$

where the nonvanishing building blocks of ρ_0 are listed in Eqs. (2.32)–(2.48). The matrix ρ^{rest} is also decomposed according to Eq. (2.26) with matrices $\rho_Y^{X,\text{rest}}$ expanded like in Eqs. (2.25), (2.28). The nonvanishing entries of the various matrices $\rho_Y^{X,\text{rest}}$ that make up ρ^{rest} read (we suppress here the index ''rest'' for aesthetic reasons)

$$a_{VV}^{PC}=(1+z^2)l_1, \tag{3.11}$$

$$b_{3,VV}^{\pm,PC}=-\kappa\pi r\beta z\sqrt{1-z^2}, \tag{3.12}$$

$$c_{0,VV}^{PC}=-(1-z^2)l_1, \tag{3.13}$$

$$c_{4,VV}^{PC}=2l_1, \tag{3.14}$$

$$c_{5,VV}^{PC}=2[1+(1-r)z^2]l_1, \tag{3.15}$$

$$c_{6,VV}^{PC}=-z(2-r)l_1, \tag{3.16}$$

$$b_{1,VV}^{\pm,PV}=rl_1, \tag{3.17}$$

$$b_{2,VV}^{\pm,PV}=z(2-r)l_1, \tag{3.18}$$

$$c_{8,VV}^{PV}=-\kappa\pi r\beta\sqrt{1-z^2}, \tag{3.19}$$

$$a_{AA}^{PC}=(1+z^2)l_2, \tag{3.20}$$

$$c_{0,AA}^{PC}=(1-z^2)l_2, \tag{3.21}$$

$$c_{4,AA}^{PC}=-2l_2, \tag{3.22}$$

$$c_{6,AA}^{PC}=2zl_2, \tag{3.23}$$

$$b_{2,AA}^{\pm,PV}=2zl_2, \tag{3.24}$$

$$b_{1,VA_+}^{\pm,PC}=-zr(\beta^2-2)l_3, \tag{3.25}$$

$$b_{2,VA_+}^{\pm,PC}=[2(1+z^2)+r(\beta^2-2)z^2]l_3, \tag{3.26}$$

$$c_{7,VA_+}^{PC}=-2\kappa\pi(1-\beta^2)\sqrt{1-z^2}, \tag{3.27}$$

$$c_{8,VA_+}^{PC}=\kappa\pi z[2(1-\beta^2)+(\beta^2-2)r]\sqrt{1-z^2}, \tag{3.28}$$

$$a_{VA_+}^{PV}=4zl_3, \tag{3.29}$$

$$b_{3,VA_+}^{\pm,PV}=\kappa\pi r(\beta^2-2)\sqrt{1-z^2}, \tag{3.30}$$

$$c_{5,VA_+}^{PV}=2z[r(\beta^2-2)+2]l_3, \tag{3.31}$$

$$c_{6,VA_+}^{PV}=-r(\beta^2-2)l_3. \tag{3.32}$$

For a given observable, the contributions from gluons with energy $E_g>x_{\min}\sqrt{s}/2$ are calculated by a numerical integration over the hard gluon region of the three-body phase space. The spin density matrix $\rho^{\text{hard}}(e^+e^-\to t\bar{t}g)$ for the hard gluon emission process is obtained by evaluating the left-hand side of Eq. (2.24) for $X=g$. The individual matrices $\rho_Y^{X,\text{hard}}$ are rather lengthy and we do not list them in this paper. We just mention here that instead of the expansion (2.28) of $\mathbf{B}^{\pm}$, C_{ij} with respect to $\hat{\mathbf{p}}$, $\hat{\mathbf{k}}$, and $\hat{\mathbf{n}}$ that was used for the two-parton final state, we found it more convenient for the three-parton final state in the hard gluon region to use as basis vectors $\mathbf{k}_t/|\mathbf{k}_t|$, $\mathbf{k}_{\bar{t}}/|\mathbf{k}_{\bar{t}}|$, and $(\mathbf{k}_t\times\mathbf{k}_{\bar{t}})/|\mathbf{k}_t\times\mathbf{k}_{\bar{t}}|$. Note that the matrix $\rho^{\text{hard}}(e^+e^-\to t\bar{t}g)$ does not contain any singularities and that the whole computation can be performed in $d=4$ dimensions.

IV. NUMERICAL RESULTS

In this section we present next-to-leading order results for expectation values of a variety of spin observables. For an observable $\mathcal{O}$ we use the notation

$$\langle\mathcal{O}\rangle=\langle\mathcal{O}\rangle_0+\frac{\alpha_s}{\pi}\langle\mathcal{O}\rangle_1+O\left(\frac{\alpha_s^2}{\pi^2}\right), \tag{4.1}$$

$$\sigma=\sigma_0+\frac{\alpha_s}{\pi}\sigma_1+O\left(\frac{\alpha_s^2}{\pi^2}\right), \tag{4.2}$$

where σ is the total cross section for $e^+e^-\to t\bar{t}X$ and

$$\langle\mathcal{O}\rangle_0=\frac{1}{\sigma_0}\frac{1}{2s}\int dR_2\,\text{Tr}\{\rho_0\mathcal{O}\}, \tag{4.3}$$

TABLE I. Expectation values of the observables listed in Eqs. (4.6)–(4.20) in terms of the quantities $\langle \mathcal{O}_i \rangle_{0,1}$ as defined in Eqs. (4.1)–(4.4) for different c.m. energies, $\lambda_+ = 0$ and $\lambda_- = 0, \pm 1$. For the expectation values not listed in the table we have, as discussed in the text, $\langle \bar{\mathcal{O}}_{1,3} \rangle = \langle \mathcal{O}_{1,3} \rangle$ and $\langle \mathcal{O}_{5,6} \rangle = 0$.

		c.m. energy in GeV							
		400		500		800		1000	
	λ_-	$\langle \mathcal{O}_i \rangle_0$	$\langle \mathcal{O}_i \rangle_1$	$\langle \mathcal{O}_i \rangle_0$	$\langle \mathcal{O}_i \rangle_1$	$\langle \mathcal{O}_i \rangle_0$	$\langle \mathcal{O}_i \rangle_1$	$\langle \mathcal{O}_i \rangle_0$	$\langle \mathcal{O}_i \rangle_1$
	−	−0.4870	0.039	−0.4608	0.125	−0.4014	0.309	−0.3760	0.377
$\langle \mathcal{O}_1 \rangle$	0	−0.2048	0.024	−0.1867	0.064	−0.1554	0.133	−0.1438	0.156
	+	0.4811	−0.052	0.4499	−0.139	0.3895	−0.302	0.3654	−0.363
	−	−0.1686	−0.191	−0.2578	−0.216	−0.3397	−0.118	−0.3581	−0.059
$\langle \mathcal{O}_2 \rangle$	0	−0.0583	−0.065	−0.0870	−0.070	−0.1120	−0.036	−0.1173	−0.017
	+	0.2099	0.225	0.3094	0.228	0.3927	0.102	0.4104	0.040
	−	−0.1686	−0.185	−0.2578	−0.165	−0.3397	0.113	−0.3581	0.267
$\langle \bar{\mathcal{O}}_2 \rangle$	0	−0.0583	−0.063	−0.0870	−0.053	−0.1120	0.040	−0.1173	0.090
	+	0.2099	0.218	0.3094	0.167	0.3927	−0.165	0.4104	−0.334
	−	0	−0.332	0	−0.232	0	−0.121	0	−0.093
$\langle \mathcal{O}_3 \rangle$	0	0	−0.356	0	−0.246	0	−0.127	0	−0.097
	+	0	−0.413	0	−0.279	0	−0.140	0	−0.106
	−	0.25	−0.015	0.25	−0.087	0.25	−0.310	0.25	−0.418
$\langle \mathcal{O}_4 \rangle$	0	0.25	−0.015	0.25	−0.086	0.25	−0.307	0.25	−0.414
	+	0.25	−0.015	0.25	−0.084	0.25	−0.300	0.25	−0.405
	−	0	−0.002	0	−0.016	0	−0.062	0	−0.082
$\langle \mathcal{O}_7 \rangle$	0	0	−0.002	0	−0.017	0	−0.065	0	−0.086
	+	0	−0.003	0	−0.019	0	−0.071	0	−0.094
	−	0.2392	−0.033	0.2240	−0.095	0.2006	−0.224	0.1927	−0.280
$\langle \mathcal{O}_8 \rangle$	0	0.2375	−0.037	0.2205	−0.100	0.1957	−0.225	0.1876	−0.278
	+	0.2332	−0.046	0.2123	−0.111	0.1848	−0.225	0.1765	−0.272
	−	0.1173	0.039	0.1606	0.030	0.2128	−0.142	0.2258	−0.244
$\langle \mathcal{O}_9 \rangle$	0	0.1182	0.041	0.1620	0.031	0.2137	−0.143	0.2265	−0.246
	+	0.1206	0.045	0.1652	0.032	0.2157	−0.147	0.2279	−0.249
	−	0.1580	0.162	0.2191	0.107	0.2442	−0.141	0.2417	−0.247
$\langle \mathcal{O}_{10} \rangle$	0	0.1693	0.170	0.2323	0.106	0.2560	−0.155	0.2528	−0.264
	+	0.1968	0.189	0.2630	0.102	0.2823	−0.187	0.2770	−0.303
	−	0	0.330	0	0.222	0	0.097	0	0.066
$\langle \mathcal{O}_{11} \rangle$	0	0	0.114	0	0.075	0	0.032	0	0.022
	+	0	−0.410	0	−0.266	0	−0.112	0	−0.076
	−	0	0.181	0	0.225	0	0.189	0	0.160
$\langle \mathcal{O}_{12} \rangle$	0	0	0.077	0	0.093	0	0.076	0	0.064
	+	0	−0.177	0	−0.213	0	−0.174	0	−0.146

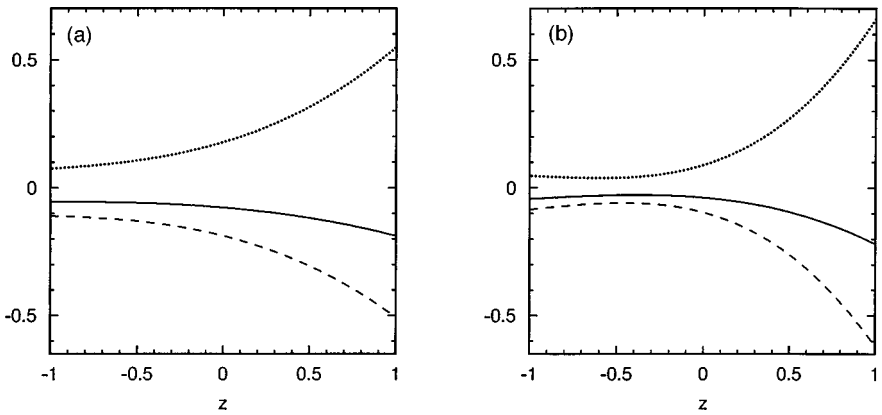

FIG. 1. Expectation value $\langle \mathcal{O}_1 \delta(z - z') \rangle$ to order α_s for a fixed value $\alpha_s = 0.1$ and $\lambda_+ = 0$. In (a) (b) the c.m. energy is set to $\sqrt{s} = 500$ GeV ($\sqrt{s} = 1$ TeV). The solid line is the result for $\lambda_- = 0$, the dashed line for $\lambda_- = -1$, and the dotted line for $\lambda_- = +1$.

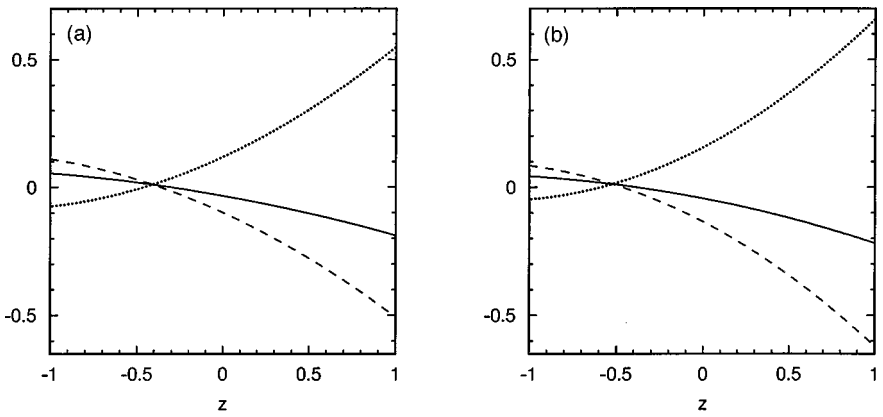

FIG. 2. Same as Fig. 1, but for $\langle \mathcal{O}_2 \delta(z-z') \rangle$.

$$\langle \mathcal{O} \rangle_1 = \frac{1}{\sigma_0} \frac{1}{2s} \left[\int dR_2 \mathrm{Tr}\{ \lim_{\epsilon \to 0} (\rho^{\mathrm{soft}} + \rho^{\mathrm{virtual}}) \mathcal{O} \} + \int dR_3 \Theta(E_g - x_{\min} \sqrt{s}/2) \mathrm{Tr}\{ \rho^{\mathrm{hard}} \mathcal{O} \} \right] - \langle \mathcal{O} \rangle_0 \frac{\sigma_1}{\sigma_0}. \tag{4.4}$$

Here, dR_2 is given in Eq. (2.50) and

$$dR_3 = \frac{d^3 k_t}{(2\pi)^3 2k_t^0} \frac{d^3 k_{\bar{t}}}{(2\pi)^3 2k_{\bar{t}}^0} \frac{d^3 k_g}{(2\pi)^3 2k_g^0} (2\pi)^4 \times \delta(p_+ + p_- - k_t - k_{\bar{t}} - k_g). \tag{4.5}$$

We consider the following set of observables:

$$\mathcal{O}_1 = \hat{\mathbf{p}} \cdot \mathbf{S}_t, \tag{4.6}$$

$$\overline{\mathcal{O}_1} = \hat{\mathbf{p}} \cdot \mathbf{S}_{\bar{t}}, \tag{4.7}$$

$$\mathcal{O}_2 = \hat{\mathbf{k}} \cdot \mathbf{S}_t, \tag{4.8}$$

$$\overline{\mathcal{O}_2} = \hat{\mathbf{k}} \cdot \mathbf{S}_{\bar{t}}, \tag{4.9}$$

$$\mathcal{O}_3 = \hat{\mathbf{n}} \cdot \mathbf{S}_t, \tag{4.10}$$

$$\overline{\mathcal{O}_3} = \hat{\mathbf{n}} \cdot \mathbf{S}_{\bar{t}}, \tag{4.11}$$

$$\mathcal{O}_4 = \mathbf{S}_t \cdot \mathbf{S}_{\bar{t}}, \tag{4.12}$$

$$\mathcal{O}_5 = \hat{\mathbf{p}} \cdot (\mathbf{S}_t \times \mathbf{S}_{\bar{t}}), \tag{4.13}$$

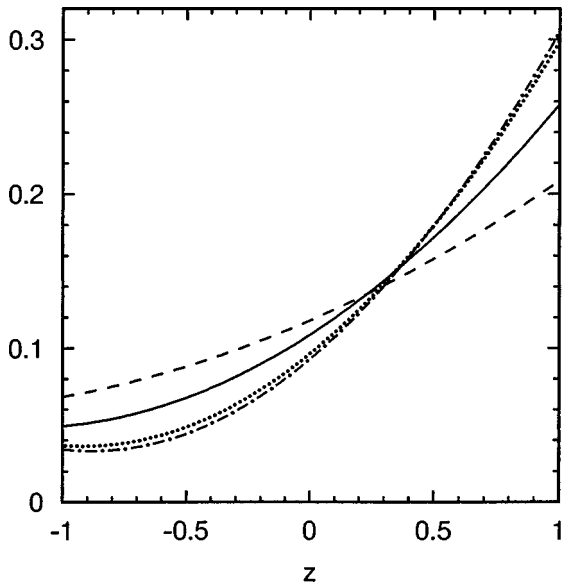

FIG. 3. Expectation value $\langle \mathcal{O}_4 \delta(z-z') \rangle$ to order α_s for a fixed value $\alpha_s = 0.1$, $\lambda_+ = \lambda_- = 0$, and c.m. energies $\sqrt{s} = 400$ GeV (dashed line), $\sqrt{s} = 500$ GeV (solid line), $\sqrt{s} = 800$ GeV (dotted line), and $\sqrt{s} = 1000$ GeV (dash-dotted line).

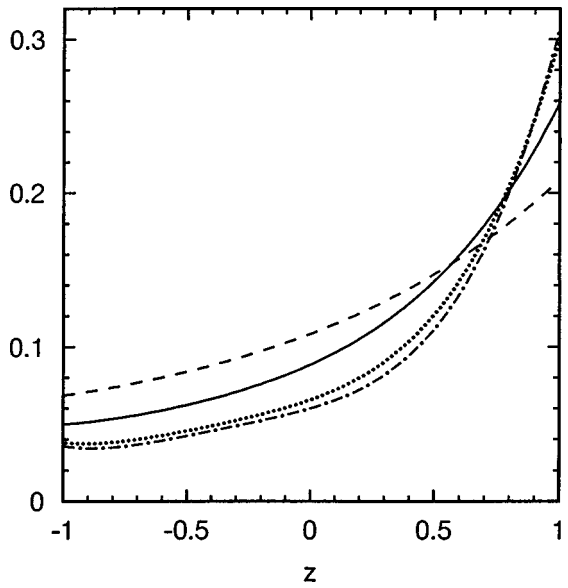

FIG. 4. Same as Fig. 3, but for $\langle \mathcal{O}_8 \delta(z-z') \rangle$.

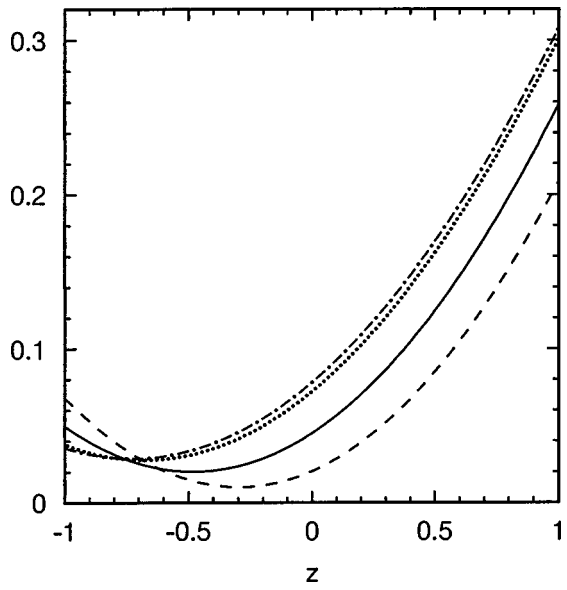

FIG. 5. Same as Fig. 3, but for $\langle \mathcal{O}_9 \delta(z-z') \rangle$.

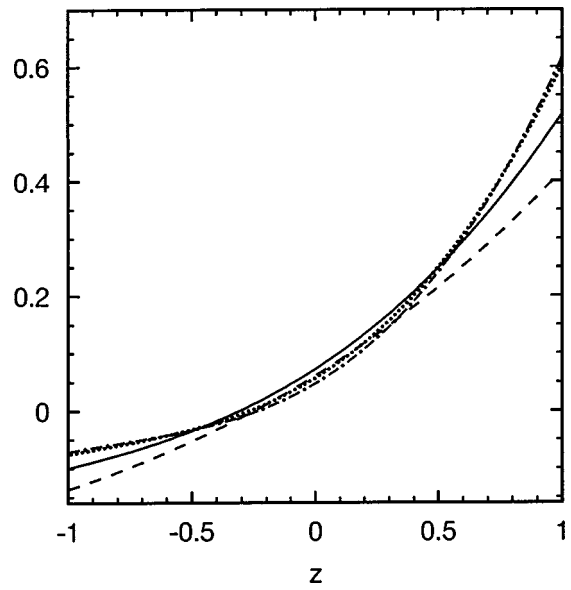

FIG. 6. Same as Fig. 3, but for $\langle \mathcal{O}_{10} \delta(z-z') \rangle$.

$$\mathcal{O}_6 = \hat{\mathbf{k}} \cdot (\mathbf{S}_t \times \mathbf{S}_{\bar{t}}), \tag{4.14}$$

$$\mathcal{O}_7 = \hat{\mathbf{n}} \cdot (\mathbf{S}_t \times \mathbf{S}_{\bar{t}}), \tag{4.15}$$

$$\mathcal{O}_8 = (\hat{\mathbf{p}} \cdot \mathbf{S}_t)(\hat{\mathbf{p}} \cdot \mathbf{S}_{\bar{t}}), \tag{4.16}$$

$$\mathcal{O}_9 = (\hat{\mathbf{k}} \cdot \mathbf{S}_t)(\hat{\mathbf{k}} \cdot \mathbf{S}_{\bar{t}}), \tag{4.17}$$

$$\mathcal{O}_{10} = (\hat{\mathbf{p}} \cdot \mathbf{S}_t)(\hat{\mathbf{k}} \cdot \mathbf{S}_{\bar{t}}) + (\hat{\mathbf{k}} \cdot \mathbf{S}_t)(\hat{\mathbf{p}} \cdot \mathbf{S}_{\bar{t}}), \tag{4.18}$$

$$\mathcal{O}_{11} = (\hat{\mathbf{p}} \cdot \mathbf{S}_t)(\hat{\mathbf{n}} \cdot \mathbf{S}_{\bar{t}}) + (\hat{\mathbf{n}} \cdot \mathbf{S}_t)(\hat{\mathbf{p}} \cdot \mathbf{S}_{\bar{t}}), \tag{4.19}$$

$$\mathcal{O}_{12} = (\hat{\mathbf{k}} \cdot \mathbf{S}_t)(\hat{\mathbf{n}} \cdot \mathbf{S}_{\bar{t}}) + (\hat{\mathbf{n}} \cdot \mathbf{S}_t)(\hat{\mathbf{k}} \cdot \mathbf{S}_{\bar{t}}). \tag{4.20}$$

The expectation values $\langle \mathcal{O}_2 \rangle_0$ and $\langle \mathcal{O}_9 \rangle_0$ are given in analytic form in Eqs. (2.54) and (2.55), respectively.

Several constraints are imposed by discrete symmetries on the expectation values of the observables (4.6)–(4.20). An unpolarized e^+e^- initial state is an eigenstate of the combined charge conjugation (C) and parity (P) transformation. CP invariance of the interactions considered here then implies $\langle \mathcal{O}_1 \rangle = \langle \bar{\mathcal{O}}_1 \rangle$ and $\langle \mathcal{O}_5 \rangle = 0$. Further, differences between $\langle \mathcal{O}_2 \rangle$ and $\langle \bar{\mathcal{O}}_2 \rangle$ as well as nonzero values for $\langle \mathcal{O}_6 \rangle$ and $\langle \mathcal{O}_7 \rangle$ can only be generated by the contributions from hard gluon emission, since $\mathbf{S}_t \overset{CP}{\to} \mathbf{S}_{\bar{t}}$, $\mathbf{k}_t \overset{CP}{\to} -\mathbf{k}_{\bar{t}}$, and since we have $\mathbf{k}_{\bar{t}} = -\mathbf{k}_t$ for a final state consisting solely of a $t\bar{t}$ pair (recall that the three-momenta are defined in the e^+e^- c.m. system). From invariance under the time reversal operation T it follows that nonzero $\langle \mathcal{O}_3 \rangle$, $\langle \bar{\mathcal{O}}_3 \rangle$, $\langle \mathcal{O}_6 \rangle$, $\langle \mathcal{O}_{11} \rangle$, and $\langle \mathcal{O}_{12} \rangle$ can only be generated by absorptive parts in the scattering amplitude. To order α_s this means that $\langle \mathcal{O}_6 \rangle$ is exactly zero due to CP invariance, while $\langle \mathcal{O}_3 \rangle = \langle \bar{\mathcal{O}}_3 \rangle$, $\langle \mathcal{O}_{11} \rangle$, and $\langle \mathcal{O}_{12} \rangle$ get nonzero, albeit small, contributions from the imaginary parts

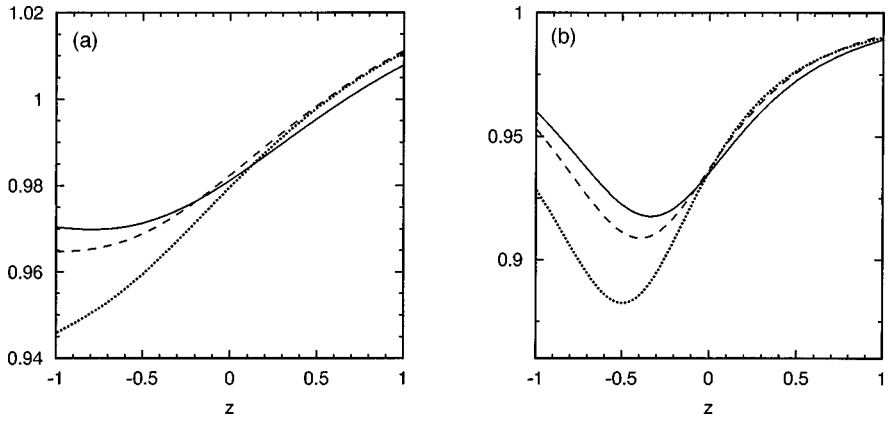

FIG. 7. The function $K_1(z)$ defined in Eq. (4.23). In (a) (b) the c.m. energy is set to $\sqrt{s} = 500$ GeV ($\sqrt{s} = 1$ TeV). The solid line is the result for $\lambda_- = 0$, the dashed line for $\lambda_- = -1$, and the dotted line for $\lambda_- = +1$.

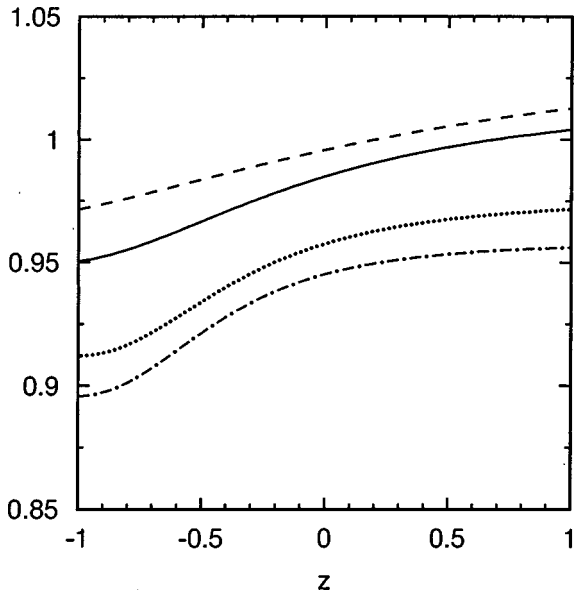

FIG. 8. The function $K_4(z)$ defined in Eq. (4.23) for $\lambda_+=\lambda_-=0$ and c.m. energies $\sqrt{s}=400$ GeV (dashed line), $\sqrt{s}=500$ GeV (solid line), $\sqrt{s}=800$ GeV (dotted line), and $\sqrt{s}=1000$ GeV (dash-dotted line).

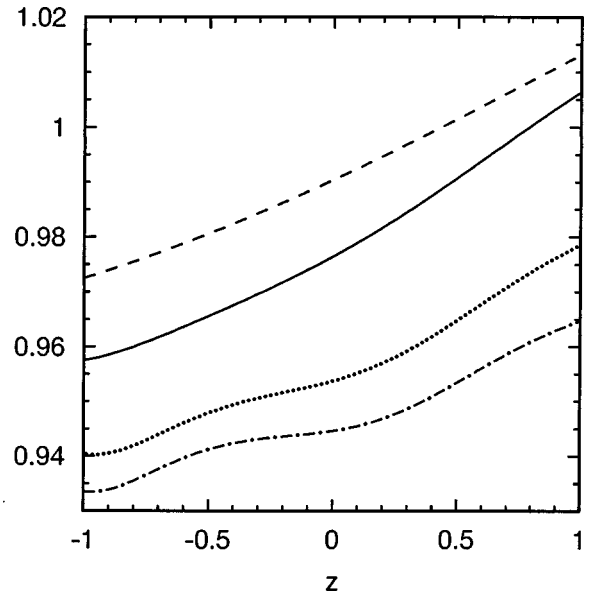

FIG. 9. Same as Fig. 8, but for $K_8(z)$.

of the one-loop integrals appearing in the virtual corrections [cf. the functions $b^{\pm,PC}_{3,VV}$, $b^{\pm,PV}_{3,VA_+}$, and $c^{PV}_{8,VV}$, $c^{PC}_{7,8,VA_+}$ in Eqs. (3.12),(3.30),(3.19),(3.27),(3.28), respectively]. All the above arguments also hold for the case of polarized electrons (and/or positrons), although in that case the initial state has no definite CP parity. This is because the net effect of a CP transformation of the initial state is $\lambda_{\mp}\to-\lambda_{\pm}$ in our formulas, and hence the couplings g^X_Y are left unchanged [cf. Eqs. (2.13)–(2.22)].

In Table I we list our results for the expectation values of Eqs. (4.6)–(4.20) in terms of the quantities $\langle\mathcal{O}_i\rangle_{0,1}$ as defined in Eqs. (4.1)–(4.4). We choose four different c.m. energies, namely $\sqrt{s}=400$, 500, 800, and 1000 GeV. The positron beam is always assumed to be unpolarized, while for the electron beam the three cases $\lambda_-=0,\pm1$ are considered. As numerical input we use $m_Z=91.187$ GeV, an on-shell top quark mass of $m=175$ GeV, and $\sin^2\vartheta_W=0.2236$.

The table shows that the top quark and antiquark are produced highly polarized and also that the spin-spin correlations are large. For example, the polarization[5] of the top quark projected onto the beam axis at $\sqrt{s}=500$ GeV and for $\lambda_-=+1$ amounts to

$$2\langle\hat{\mathbf{p}}\cdot\mathbf{S}_t\rangle=0.8998-0.278\,\frac{\alpha_s}{\pi}=0.8910, \qquad (4.21)$$

where we set $\alpha_s=0.1$. As another example, consider the spin-spin correlation $\langle\mathcal{O}_{10}\rangle$ at $\sqrt{s}=1$ TeV, also for $\lambda_-=+1$:

$$\langle(\hat{\mathbf{p}}\cdot\mathbf{S}_t)(\hat{\mathbf{k}}\cdot\mathbf{S}_{\bar{t}})+(\hat{\mathbf{k}}\cdot\mathbf{S}_t)(\hat{\mathbf{p}}\cdot\mathbf{S}_{\bar{t}})\rangle$$
$$=0.2770-0.303\,\frac{\alpha_s}{\pi}=0.2674, \qquad (4.22)$$

where we again set $\alpha_s=0.1$.

A global characteristic of all the expectation values of the observables (4.6)–(4.20) is that the QCD corrections are quite small. The quantity $\alpha_s/\pi\times|\langle\mathcal{O}_i\rangle_1/\langle\mathcal{O}_i\rangle_0|$ ranges, for nonzero $\langle\mathcal{O}_i\rangle_0$ and (a fixed value of) $\alpha_s=0.1$, between 1.9 per mil (for $\langle\mathcal{O}_4\rangle$ at $\sqrt{s}=400$ GeV and all three choices of λ_-) and 5.3% (amusingly also for $\langle\mathcal{O}_4\rangle$, but at $\sqrt{s}=1000$ GeV and $\lambda_-=-1$).[6]

To check our calculation, we compared our numerical value for the order α_s correction to the total cross section σ_1 with the value one gets by using the analytic formula as given for example in [16] and found excellent agreement. Note that the longitudinal spin-spin correlation $\langle P^{ll}\rangle$ studied in [8] is, at next-to-leading order, *not* proportional to our expectation value $\langle\mathcal{O}_9\rangle$: The former would correspond in our notation to the expectation value $4\langle(\hat{\mathbf{k}}_t\cdot\mathbf{S}_t)(\hat{\mathbf{k}}_{\bar{t}}\cdot\mathbf{S}_{\bar{t}})\rangle$, which only at leading order is equal to $-4\langle\mathcal{O}_9\rangle$. To compare our results for $\langle P^{ll}\rangle$, we reproduced Figs. 1 and 2 of Ref. [8] and found agreement.

We now study the distributions of our expectation values with respect to z, the cosine of the top quark scattering angle in the c.m. system. These distributions are defined as $\langle\mathcal{O}_i\delta(z-z')\rangle$; i.e., we do not average over z but over all other kinematic variables.

The distributions $\langle\mathcal{O}_{3,11,12}\delta(z-z')\rangle$ are not shown, since they can be easily constructed from the listed analytic formulas for $b^{\pm}_3, c_{7,8}$. We also do not show the distribution

[5]The polarization is conventionally defined as *2 times* the expectation value of the spin operator.

[6]At leading order, $\langle\mathcal{O}_4\rangle=1/4$, since the reaction proceeds through a single spin-1 boson.

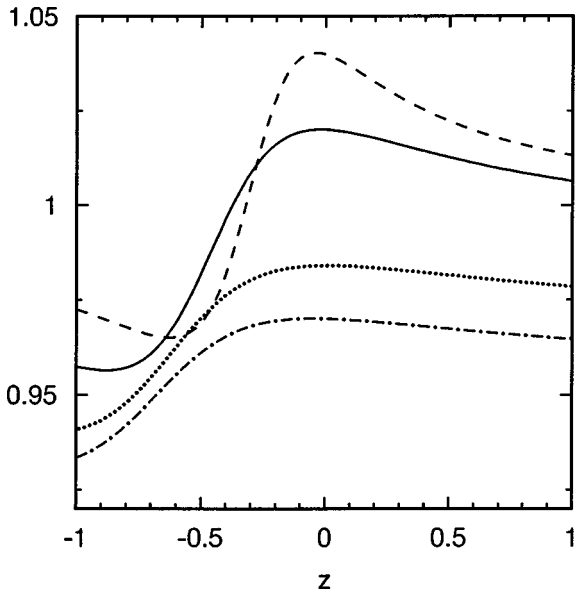

FIG. 10. Same as Fig. 8, but for $K_9(z)$.

$\langle \mathcal{O}_7 \delta(z-z') \rangle$, since according to Table I the expectation value $\langle \mathcal{O}_7 \rangle$ varies (again for a fixed $\alpha_s = 0.1$) between the tiny values -0.6×10^{-4} and -0.3%.

Figures 1(a) and 1(b) show, to NLO accuracy, the distribution $\langle \mathcal{O}_1 \delta(z-z') \rangle$ at c.m. energies $\sqrt{s} = 500$ GeV and $\sqrt{s} = 1$ TeV, respectively, for $\lambda_- = 0, \pm 1$. In this and all the following plots we set $\alpha_s = 0.1$. Note that the distribution gets more peaked near $z = +1$ as the c.m. energy rises. This feature is less pronounced in the distribution $\langle \mathcal{O}_2 \delta(z-z') \rangle$ depicted in Figs. 2(a),2(b). In Figs. 3–6 we show the distributions for different spin-spin correlations, namely $\langle \mathcal{O}_{4,8,9,10} \delta(z-z') \rangle$. In these figures, the c.m. energy is varied between $\sqrt{s} = 400$ GeV and $\sqrt{s} = 1$ TeV, while the electron polarization is set to $\lambda_- = 0$. The results for other choices of λ_- do not differ much from the ones shown. This is also reflected in the rather weak dependence of the spin-spin correlations $\langle \mathcal{O}_{4,8,9,10} \rangle$ on λ_- (cf. Table I). Note that the distributions typically rise as $z \to +1$.

To illustrate the impact of the $O(\alpha_s)$ corrections, we plot in Figs. 7–10 the ''K-factors''

$$K_i(z) = \frac{\langle \mathcal{O}_i \delta(z-z') \rangle_0 + \alpha_s/\pi \langle \mathcal{O}_i \delta(z-z') \rangle_1}{\langle \mathcal{O}_i \delta(z-z') \rangle_0} \quad (4.23)$$

for $i = 1$ [Figs. 7(a),7(b)], and $i = 4,8,9$ (Figs. 8,9,10). The K-factors show a strong dependence both on the cosine of the scattering angle and on the c.m. energy. They vary between 0.88 and 1.04.

V. CONCLUSIONS

The production of top quark pairs in e^+e^- annihilation involves a variety of spin phenomena. We have performed a systematic study of these effects to order α_s and including beam polarization effects using the spin density matrix formalism. Apart from a significant polarization of the top quarks and antiquarks, the spins of t and $\bar{t}$ are also strongly correlated. The QCD corrections to the leading order results for the expectation values of all spin observables considered are at the percent level or smaller. The spin effects in the $t\bar{t}$ production will manifest themselves in the angular distributions of the t and $\bar{t}$ decay products. For a phenomenological analysis of these angular distributions, one can combine the results presented in this paper with spin decay matrices computed to next-to-leading order accuracy for the different t and $\bar{t}$ decay modes.

ACKNOWLEDGMENTS

We would like to thank W. Bernreuther for many enlightening discussions and for his comments on the manuscript. This work was supported by BMBF, contract 057AC9EP. A.B. was supported by Deutsche Forschungsgemeinschaft.

[1] E. Accomando *et al.*, Phys. Rep. **299**, 1 (1998).
[2] J. H. Kühn, A. Reiter, and P. M. Zerwas, Nucl. Phys. **B272**, 560 (1986).
[3] S. Parke and Y. Shadmi, Phys. Lett. B **387**, 199 (1996).
[4] J. G. Körner, A. Pilaftsis, and M. M. Tung, Z. Phys. C **63**, 575 (1994); M. M. Tung, Phys. Rev. D **52**, 1353 (1995).
[5] S. Groote and J. G. Körner, Z. Phys. C **72**, 255 (1996).
[6] W. Bernreuther, J. P. Ma, and T. Schröder, Phys. Lett. B **297**, 318 (1992).
[7] M. M. Tung, J. Bernabeu, and J. Penarrocha, Phys. Lett. B **418**, 181 (1998).
[8] S. Groote, J. G. Körner, and J. A. Leyva, Phys. Lett. B **418**, 192 (1998).
[9] R. Harlander, M. Jezabek, J. H. Kühn, and T. Teubner, Phys. Lett. B **346**, 137 (1995).
[10] A. Czarnecki, M. Jezabek, and J. H. Kühn, Nucl. Phys. **B351**, 70 (1991).
[11] B. Lampe, Report No. MPI-PHT-98-07, hep-ph/9801346.
[12] C. Schmidt, Phys. Rev. D **54**, 3250 (1996).
[13] W. Bernreuther, O. Nachtmann, P. Overmann, and T. Schröder, Nucl. Phys. **B388**, 53 (1992); **B406**, 516(E) (1993).
[14] G. 't Hooft and M. Veltman, Nucl. Phys. **B44**, 189 (1972).
[15] S. A. Larin, Phys. Lett. B **303**, 113 (1993).
[16] K. G. Chetyrkin, J. H. Kühn, and A. Kwiatkowski, Phys. Rep. **277**, 189 (1996).